The sub-seasonal and interannual spatio-temporal variability of bare-ice albedo of Abramov Glacier, Kyrgyzstan

Anouk VOLERY[1,2], Kathrin NAEGELI[2,*], Martina BARANDUN[1,*]

[1]*Department of Geosciences, University of Fribourg, Fribourg, Switzerland*

[2]*Department of Geography, Remote Sensing Laboratories, University of Zurich, Zurich, Switzerland*

*These authors contributed equally to this work.

ABSTRACT.

As snowlines retreat, the bare ice of Central Asian glaciers is increasingly exposed to short-wave radiation and high temperatures. The importance of bare-ice albedo for glacier melt rates is thus rising. Little is known about the variability of bare-ice albedo, its drivers or its implications for glacier melt. We address this gap by presenting the sub-seasonal and inter-annual variability of bare-ice albedo of Abramov Glacier in Kyrgyzstan between 1999 and 2022. We derived albedo products from Landsat surface reflectance data, investigated the relationship between air temperature and bare-ice albedo variability and explored the implications of this variability for glacier melt. Our results indicate that bare-ice albedo undergoes a sub-seasonal cycle controlled by air temperature and elevation-dependant refreezing events. Bare-ice albedo decreased over the tongue in July and August between 1999 and 2017, while, in 2018, a lateral displacement of the ice resulted in a shift in the patterns of bare-ice albedo. We found significant correlations between bare-ice albedo variability and both temperature and glacier melt at various timescales. Rising temperatures are thus expected to lead to darker bare ice and amplified feedback melt cycles. Integrating albedo variability into glaciological models is thus crucial for accurate predictions of accelerated glacier response to intensifying climate change.

INTRODUCTION

In a warming climate, snowlines retreat earlier in the season and to higher elevations (Oerlemans, 2001). As a result, more bare ice is becoming exposed at the glacier surface and for longer periods of time (Box and others, 2012; Di Mauro and Fugazza, 2022). This growing exposure has implications for the surface energy balance and melting rates (Hartl and others, 2020; Di Mauro and Fugazza, 2022; Gunnarsson and Gardarsson, 2023). Radiative transfers control the surface energy balance (Greuell and Smeets, 2001; Klok and Oerlemans, 2002) and, among these transfers, short-wave radiation is usually the dominant energy source for extra-tropical glaciers (Braithwaite, 1995; Oerlemans, 2001; Marshall, 2014). The albedo of the exposed snow, firn and ice modulates the absorption of short-wave radiation, resulting in distinct albedo zones on glaciers. The variability of bare-ice albedo critically impacts the extent and amount of surface melt in ablation areas, where the net mass loss occurs (Hall and others, 1987; Hartl and others, 2020). Conversely, bare-ice albedo is influenced by radiative transfers, as the net energy budget alters the ice surface properties, on which albedo relies. Such feedback mechanisms generate self-feeding melt cycles and explain the amplified response of glaciers to atmospheric changes (Johnson and Rupper, 2020). Rising temperatures play a key role in these melt cycles, as higher air temperatures enhance the energy input to the surface energy budget of ablation areas by modulating long-wave radiation and sensible heat fluxes. On bare-ice, this contributes to warmer ice, larger grain sizes and meltwater presence on the ice—all of which decrease the bare-ice albedo of glaciers (Azzoni and others, 2016; Fugazza and others, 2016; Tedstone and others, 2020). Therefore, with the increased and prolonged exposure of bare ice to rising temperatures, the influence of bare-ice albedo variability on glacier surface energy balance and melting rates is expected to grow.

Multiple studies have investigated glacier-wide albedo (Brock and others, 2000b; Jonsell and others, 2003; Gascoin and others, 2017; Marshall and Miller, 2020; Gunnarsson and others, 2021; Di Mauro and Fugazza, 2022). The temporal variability of glacier-wide albedo provides valuable information on the snow-free and snow-covered fractions of glaciers (Davaze and others, 2018). Therefore, the annual minimum albedo averaged over the glacier can be used to derive the annual equilibrium line altitude (ELA) (Brun and others, 2015; Shaw and others, 2021). However, the temporal variability of glacier-wide albedo does not capture the variability of albedo of the bare-ice that remains exposed during ablation season. This variability significantly impacts glacier melt, as Naegeli and Huss (2017) found an average decrease of -0.14 m w.e. a $^{-1}$ in the mass balance of 12 Swiss glaciers for every 0.1 reduction of bare-ice albedo. A

similar sensitivity of mass balance to bare-ice albedo variability has been found for glaciers in the Chilean Andes (Barandun and others, 2022). Yet few studies have investigated this variability (Cutler and Munro, 1996; Jonsell and others, 2003; Dumont and others, 2012; Naegeli and Huss, 2017; Naegeli and others, 2019; Hartl and others, 2020; Tedstone and others, 2020; Barandun and others, 2022; Rossini and others, 2023) and bare-ice albedo is often assumed to be constant in space and time in mass balance modelling (Klok and Oerlemans, 2002; Machguth and others, 2008). A growing body of research is exploring the potential of remote sensing, in-situ measurement and unmanned aerial system (UAS) technology to monitor albedo and linked glacier surface properties (Naegeli and others, 2019; Hartl and others, 2020; Tedstone and others, 2020; Barandun and others, 2022; Gunnarsson and others, 2023; Rossini and others, 2023; Gunnarsson and Gardarsson, 2023). Mass balance models have been shown to improve when using the output of such monitoring efforts to replace constant albedo values with satellite-based spatially distributed albedo in Barandun and others (2022), Naegeli and others (2015). Still, to date, the spatio-temporal variability of bare-ice albedo has not been incorporated into such models.

A better understanding of the sub-seasonal and inter-annual spatio-temporal variability of bare-ice albedo is key to effectively integrate temporal and spatial albedo distributions into glaciological models. With this in mind, the present study aims to gain insights into the spatio-temporal variability of bare-ice albedo, along with its drivers and its influence on glacier melt. We focus on the bare-ice albedo of Abramov Glacier in Central Asia. The region has warmed by $0.37 - 0.43°C$ per decade over the period 1979–2011 (Hu and others, 2014). The number of summer days (days with daily maximum temperature $> 35°C$) has increased by more than 10 days per year between 1999–2019 compared to 1950–1979, while icing days (days with daily maximum temperature below $0°C$) have decreased by 15 days per year (Fallah and others, 2024). Simultaneously, snow melted earlier in the season in the Amu Darya River Basin from 1985 to 2008 (Zhou and others, 2017). Snow depth has also decreased by 20% in Central Asia over the past 70 years, associated with a warming of $1.2°C$ (Fallah and others, 2024). As a result of those changes, the bare ice of Central Asian glaciers is exposed to solar radiation, impurity deposition and rising temperatures for longer periods of time (Schmale and others, 2017; Zhang and others, 2020). Data are scarce for glaciers of Central Asia, but Abramov benefits from extensive meteorological and mass balance records (Hoelzle and others, 2017). Here, we explore bare-ice albedo variability using a time series of albedo scenes over the ablation area acquired during melt season (July–September) from 1999 to 2022. We investigate (1) the sub-seasonal temporal and spatial variability of bare-ice albedo of Abramov, (2) the inter-annual variability of bare-ice

albedo under the changing conditions for the period from 1999 to 2022, (3) the role of air temperature in modulating bare-ice albedo and (4) the influence of bare-ice albedo on variations of melting rates.

1 STUDY SITE

Abramov Glacier ($39.50°N, 71.55°E$) is located in the Pamir-Alay range in Kyrgyzstan, Central Asia, and feeds the Koksu river, a tributary of the Amu Darya (Denzinger and others, 2021). This is a north-facing valley glacier, with longitudinal supra-glacial medial moraines and a significant load of debris and impurities, such as light-absorbing particles and dust, on the lower tongue (Fig. 1). The glacier extends over $21.27\,km^2$ (Mattea and others, 2023) between 3650 and 5000 m a.s.l. Mass balance measurements started already in the 1960s, but the collapse of the Soviet Union brought the measurement campaigns to an end in 1999 (Suslov and Krenke, 1980; Glazyrin and others, 1993; Pertziger, 1996; Hoelzle and others, 2017; Kronenberg and others, 2021). The monitoring was re-initiated in 2011 (Hoelzle and others, 2017). An automatic weather station (AWS) and an automatic terrestrial camera (Mobotix M25) were installed at 4100 m a.s.l. about 1.5 km from the glacier terminus (Fig. 1a) (Schöne and others, 2013; Barandun and others, 2018). The mean air temperatures measured at the station from 2011 to 2022 are $5.78°C$ in July, $4.89°C$ in August, and $1.89°C$ in September.

Abramov has lost mass in recent decades. Kronenberg and others (2022) calculated a mass balance of -0.27 m w.e. a $^{-1}$ for the period 1968/69–2019/20. Concurrent with this mass loss, Kronenberg and others (2021) estimated that net accumulation had increased simultaneously to ablation over the last 60 years. The glacier has experienced occasional surge behaviour, such as between 1972 and 1975 (Emeljyanov and others, 1974; Suslov and Krenke, 1980; Glazyrin and others, 1993) and possibly in 2018 (Mattea and others, 2023, 2024). Our study area is the lower third of the glacier, covering 5.1 km^2 between 3626 and 4071 m a.s.l. In this area, bare-ice is exposed for most of summer and remains unaffected by the variations in surface types in the transition region between ablation and accumulation area.

2 DATA

Broadband albedo products

We updated the broadband albedo products derived by Barandun and others (2021) from Landsat Collection 1 and 2 Level-2 surface reflectance data from the US Geological Survey. The derivation process includes a semi-automatic classification method using the Spectral Angle Mapper (SAM) (Kruse and oth-
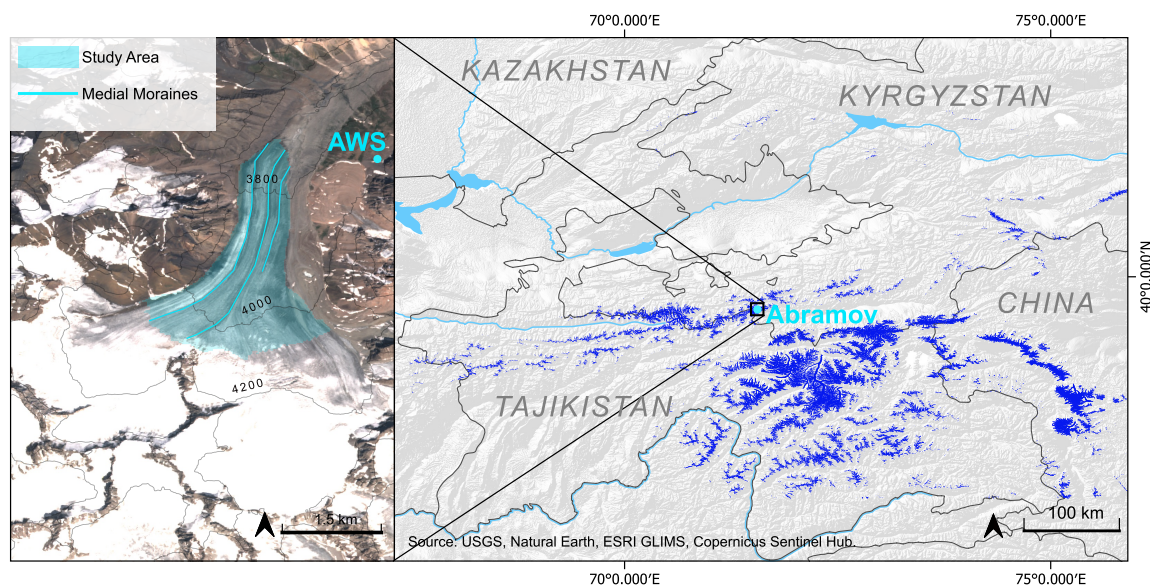
Fig. 1. Right panel: map showing the glaciated areas (dark blue) in Central Asia. Left panel: overview of Abramov glacier, on a section of a Sentinel-2 scene (20 August 2019) overlaid with elevation data from Shuttle Radar Topography Mission (SRTM) imagery. The study area is outlined (light blue), using the Global Land Ice Measurements from Space (GLIMS) dataset, modified to reflect the 2020 glacier terminus as delineated by Enrico Mattea in Mattea and others (2024). The automatic weather station (AWS) location and the manually delineated supra-glacial medial moraines are also indicated.

ers, 1993) for cloud delineation, and relies on Liang's narrow-to-broadband conversion (Liang, 2001) to derive broadband albedo from surface reflectance data. For more details on the broadband albedo derivation, please refer to Naegeli and others (2019) and Barandun and others (2021). A total of 338 scenes, with a spatial resolution of 30 m, were collected for the months of July, August and September from 1999 to 2022 and were cropped to the outlines of Abramov. The outline from the Global Land Ice Measurements from Space (GLIMS) dataset was modified to the 2020 terminus delineated by Enrico Mattea in Mattea and others (2024).

AWS data

Time series of air temperature, incoming short-wave radiation and barometric pressure were downloaded from the open-access Sensor Data Storage System (SDSS) of the AWS network provided by the Central Asia Institute of Applied Geosciences (CAIAG) and the Deutsches GeoForschungsZentrum (GFZ) Potsdam. These meteorological data were obtained for the dates on which the albedo scenes were taken and for the days preceding those dates. The time series cover the period from 20 August 2012 to 24 July 2022; a period slightly shorter than that covered by the satellite data due to the later installation of the AWS (Section 1) and partly limited by data gaps. For more information on the AWS setup, please refer to Schöne and others (2013).

Glacier melt and mass balance data

Time series of modelled cumulative daily surface melt and mass balance for 1999–2011 were provided in Barandun and others (2015), calibrated with glaciological observations and validated with snowline observations. Time series of observation-based annual surface melt and mass balance for 2012–2022 were extrapolated from point to glacier-wide mass balance following a similar approach than in Barandun and others (2015). The same model-based approach as in Barandun and others (2015) was used to derive daily mass balance and melt rates from annual observations.

Camera images

Images from the terrestrial camera (Section 1) were reviewed for the days preceding the acquisition dates of albedo scenes from 2011 to 2022. However, the series of images is discontinuous. Available images were used as qualitative control for pre-processing, such as identifying residual artifacts (sample camera imagery

is provided in Appendix A, Fig. 7).

3 METHODS

Pre-processing

We filtered the albedo scenes for bare-ice albedo (0.05–0.39) using literature-derived values adjusted with visual inspections (Paterson, 1994; Oerlemans and Knap, 1998; Cuffey and Paterson, 2010). We then validated this filtering using camera images (see Appendix A, Fig. 7), barometric pressure data and incoming short-wave radiation to detect the presence of clouds and snow on the glacier. To avoid the influence of snow and firn on the ice transitions, we focused strictly on the tongue area in the lower third of the glacier (5.2 km^2). We used elevation information from the Shuttle Radar Topography Mission (SRTM) digital elevation model (DEM) (Jarvis and others, 2008) to delineate this area. After the pre-processing, we produced two datasets: dataset 1, for a pixel-by-pixel-based analysis, included all scenes with a minimum of 20% coverage over the tongue (120 scenes); dataset 2 was specifically intended for calculation of the mean bare-ice albedo over the tongue and included all scenes with a minimum of 60% coverage over the tongue (78 scenes) (for the temporal distribution of the satellite scenes during July-August-September (JAS) over the study period (1999-2022) in dataset 1 and 2 see Appendix A, Fig. 8.

Analysis of sub-seasonal variability

For the pixel-by-pixel-based analysis, we calculated the arithmetic mean and standard deviation of bare-ice albedo for each pixel during July, August and September using dataset 1. Based on the same dataset, we averaged the difference in bare-ice albedo between July/August and August/September for each pixel. For the tongue-wide analysis, we averaged bare-ice albedo over the entire study area for each scene of dataset 2 from 1999 to 2022 and calculated the arithmetic mean for the summer (July to September) and for each individual month (July, August and September).

Analysis of inter-annual variability

We used non-parametric Mann–Kendall (MK) tests (Mann, 1945; Kendall, 1975) to detect pixel trends in the summer, July, August and September albedo time series (dataset 1). We used three confidence levels (75, 85 and 95%) to provide a comprehensive overview of changes in bare-ice albedo while maintaining robust results. We assessed the rate of albedo change using the Theil–Sen slope estimator (Theil, 1950)

for pixels with trends at 85% confidence level. In addition, we calculated the mean difference in bare-ice albedo for each pixel during July, August and September (dataset 1) of two sub-periods: 1999–2010 and 2011–2022.

Correlations of air temperature variables and bare-ice albedo

We calculated the following parameters from air temperature data for several time windows (6 h, 12 h, 24 h, 60 h, 72 h, 120 h) prior to the acquisition time of the albedo scenes: arithmetic means, nighttime minima, number of negative degree hours and number of sign changes in air temperature. We assessed the temporal relationship between the aforementioned parameters and the mean bare-ice albedo over the tongue (dataset 2) using the Kendall's tau correlation coefficients (τ) (Schaeffer and Levitt, 1956) and associated p-value.

## Correlations of melt variables and bare-ice albedo

We calculated τ coefficients and p-values between the summer, monthly and daily melt, as well as mass balance, and the mean bare-ice albedo from 1999 to 2016 (dataset 2). For the seasonal analysis, we calculated the τ and p-values between the summer surface melt, mass balance, and both the average summer albedo and the lowest mean tongue albedo. For the monthly analysis, we calculated the τ and p-values between the July, August and September surface melt and mass balance—derived from the cumulative daily data—and the corresponding average monthly albedo. For the daily analysis, we calculated the τ and p-values between the mean bare-ice albedo of each scene and the corresponding daily surface melt and mass balance—derived from cumulative daily data.

4 RESULTS

The sub-seasonal cycle of bare-ice albedo

Average bare-ice albedo at Abramov decreases from July to August and increases from August to September (Fig. 2a). The magnitude of seasonal changes in bare-ice albedo depends on elevation and presence of debris and impurities on the ice (Fig. 2b, c). From July to August, both the variability and the values of bare-ice albedo decrease significantly ($\leqslant -0.06$) at high elevation (between 3950 and 4071 m a.s.l.) on the tongue. However, bare-ice albedo remains constantly low at low elevation (between 3650 and 3850 m a.s.l.) between July and August (Fig. 2c). From August to September, the albedo of debris-free ice
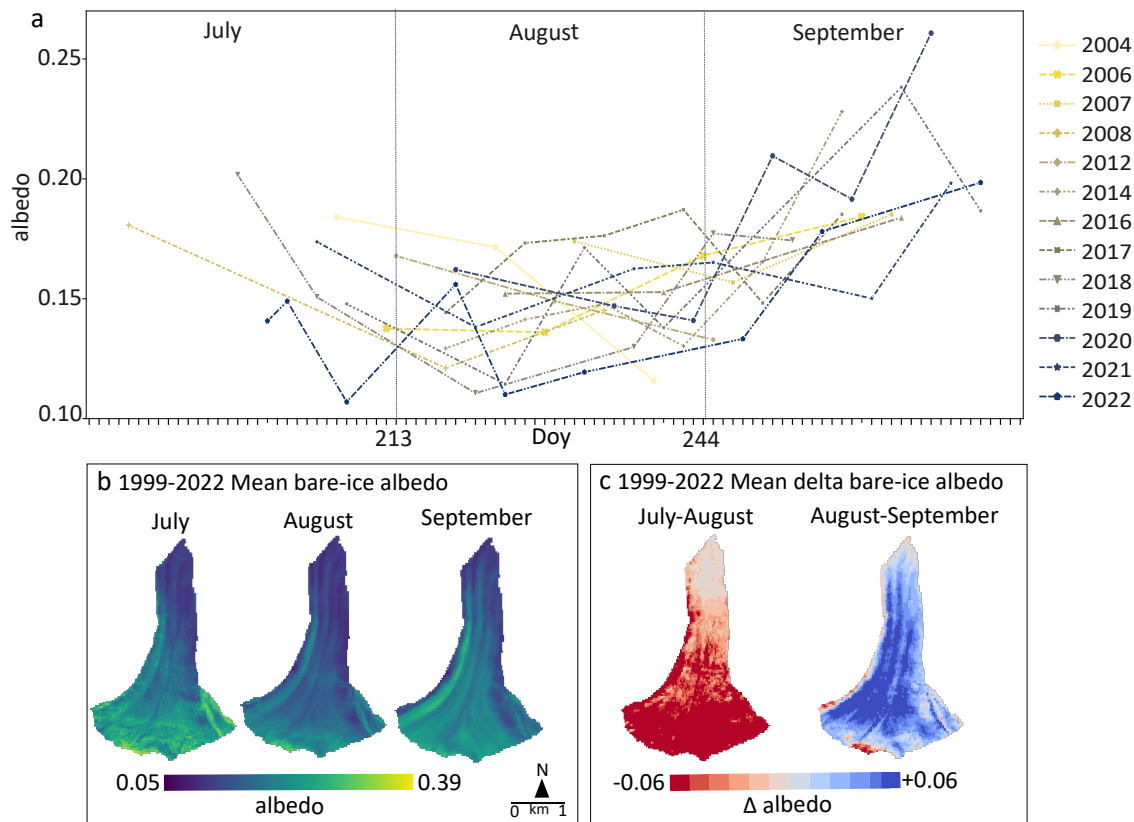
Fig. 2. (a) Time series of Abramov's average bare-ice albedo for all years with a minimum of three scenes between 1999 and 2022. (b) Spatial distribution of 1999–2022 average bare-ice albedo for July, August and September. (c) Spatial distribution of 1999–2022 average bare-ice albedo difference between July/August and August/September.

increases more significantly ($\geqslant +0.06$) than that of the ice in the area of the medial moraines (between +0.01 and +0.05; Fig. 2c).

Inter-annual variations of bare-ice albedo

Between 1999 and 2022, the bare-ice albedo decreased within the range of -0.001 to -0.01 per year over an area of 0.97 km^2 at the 95% confidence level and over 1.90 km^2 at the 75% confidence level, as shown in Fig. 3a. This slight decrease was gradual for most of the area between 1999 and 2022. However, the albedo along the eastern sides of the medial moraines decreased abruptly in 2018 and remained low afterwards, as illustrated in Fig. 3b. Conversely, the albedo along the western sides of the medial moraines increased abruptly in 2018 within the range of 0.002 to 0.006 over an area of 0.12 km^2 at the 95% confidence level and of 0.39 km^2 at the 75% confidence level, as shown in Fig. 3a, c. These small but sudden shifts in
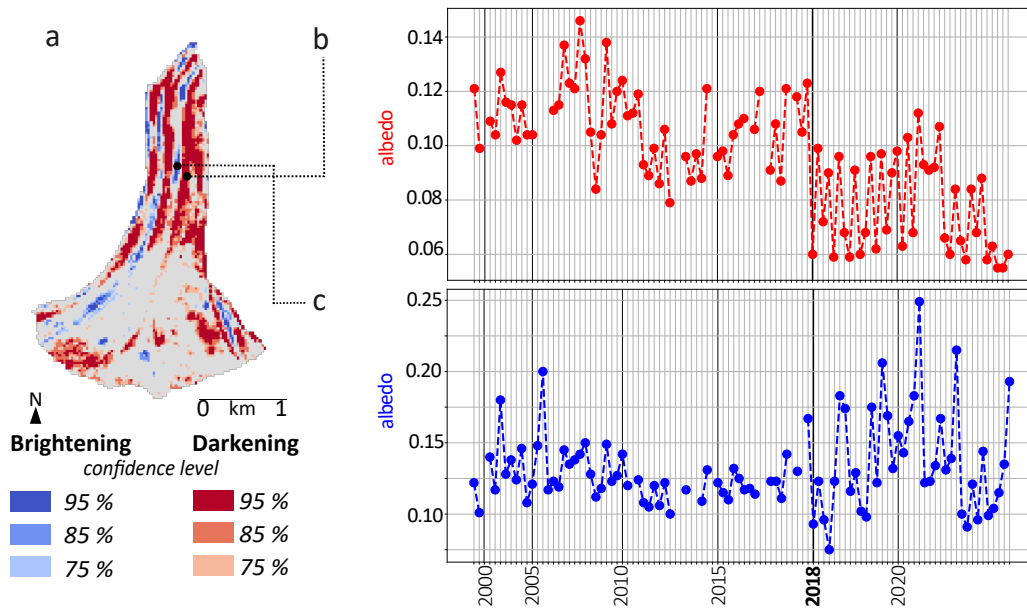
Fig. 3. (a) Spatial distribution of all significant bare-ice albedo trends (75, 85, 95% confidence level) in the 1999–2022 time series of average pixel-by-pixel summer bare-ice albedo. Bare-ice albedo time series of a pixel displaying a decreasing (b) and increasing (c) trend. For both (b) and (c) the time series include all scenes, which are in chronological but non-uniform time spacing.

bare-ice albedo values along the eastern and western margins of the medial moraines indicate a lateral ice displacement towards the east (Fig. 3a). The bare-ice albedo also decreased in July, August and September between 1999 and 2017, before the sudden shifts in bare-ice albedo values in 2018. Bare-ice albedo slightly decreased within the range of -0.002 to -0.005 per year over an area of 0.61 km^2 at the 85% confidence level in July from 1999 to 2017 and by a similar degree over an area up to 0.91 km^2 at the 85% confidence level in August (Fig. 4). Bare-ice albedo decreased over an area of 1.6 km^2 of the tongue at the 85% confidence level in September from 1999 to 2017. In September, most of the decrease in bare-ice albedo occurred at higher elevations than in July and August, where it decreased by more than -0.01 per year. Despite the overall negative trends, bare-ice albedo exhibits periods of increase in consecutive years: for example, bare-ice albedo rises in August between 2013 and 2017 within the range of 0.01 to 0.06 per year over an area of 0.41 km^2 of the tongue at the 95% confidence level and of 3.04 km^2 at the 75% confidence level.
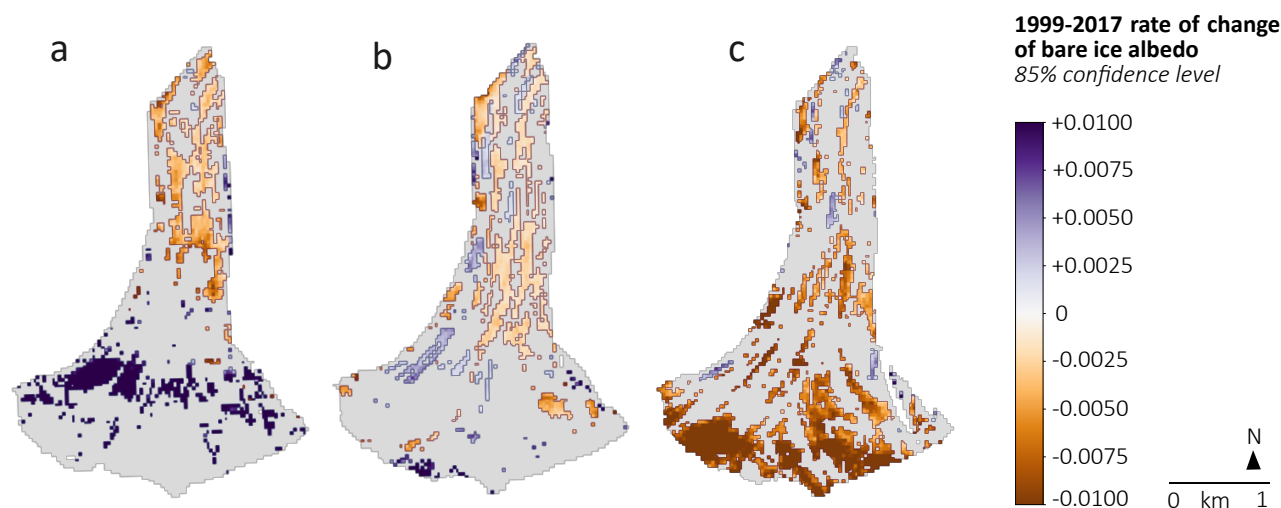
Fig. 4. The rate of change of bare-ice albedo from 1999 to 2017 for pixels showing trends at the 85% confidence level for (a) July, (b) August and (c) September.

Air temperature impact on bare-ice albedo

We detected significant correlations between all assessed air temperature parameters and mean bare-ice albedo (Table 1). Some of these correlations are illustrated by scatter plots in Appendix A, Fig. 9. Moderate negative correlations can be observed between mean bare-ice albedo and mean air temperature of the 6 h, 12 h, 24 h, 48 h, 60 h and 72 h time windows prior to albedo acquisition; the correlations are strongest with the average air temperature of the 48 h and 60 h time windows ($\tau = -0.44$). Moderate negative correlations are also present between albedo and night minimum air temperature ($\tau = -0.36$). Positive moderate correlations are apparent between bare-ice albedo and the sum of negative degree hours prior to albedo acquisition; the correlation is strongest with the sum of negative hours in the 48 h time window ($\tau = 0.45$) and in the 120 h time window ($\tau = 0.47$). Also, positive moderate correlations exist between bare-ice albedo and the sum of sign changes of air temperature (freezing/non-freezing conditions) during the time prior to albedo acquisition; the correlation is strongest with the sum of sign changes of air temperature in the 48 h time window prior to albedo acquisition ($\tau = 0.48$).

Figure 5 illustrates that high temperatures coincide with low bare-ice albedo (Fig. 5a, b, c, d), whereas low temperatures, negative degree hours and sign changes of air temperature correspond to high average

Variable (in time ranges prior to albedo acquisition)	Kendall τ
Average air temperature (6 h)	-0.38
Average air temperature (12 h)	-0.40
Average air temperature (24 h)	-0.42
Average air temperature (48 h)	-0.44
Average air temperature (60 h)	-0.44
Average air temperature (72 h)	-0.43
Nighttime min. temperature	-0.36
Sum negative degree h (12 h)	0.37
Sum negative degree h (24 h)	0.37
Sum negative degree h (48 h)	0.45
Sum negative degree h (120 h)	0.47
Sign changes of air temperature (12 h)	0.36
Sign changes of air temperature (24 h)	0.38
Sign changes of air temperature (48 h)	0.48
Sign changes of air temperature (120 h)	0.48

Table 1. Kendall τ derived between Abramov average bare-ice albedo and the following parameters: average air temperature (žC), nighttime minimum temperature (žC), the sum of negative degree hours and the sum of sign changes of air temperature for various time intervals prior to albedo acquisition. All relationships are statistically significant at the 99% confidence level with $p-values < 0.01$

bare-ice albedo (Fig. 5a, b, c, d). For example, the highest mean bare-ice albedo occurs on 23 September 2020 after 60 h of negative temperatures occurring in the last 5 days and 4 sign changes of air temperature in the past 48 h (Fig. 2d1).

Bare-ice albedo impact on glacier melt

We detected a negative correlation between the mean summer bare-ice albedo and summer melt ($\tau = -0.40$) and a moderate negative correlation between the summer minimum mean bare-ice albedo and summer melt ($\tau = -0.53$) from 1999 to 2022 (see Table 2). We also found a strong negative correlation between the summer minimum mean bare-ice albedo and summer melt ($\tau = -0.71$) from 2012 to 2022, the period during which melt was measured in-situ. Figure 6 illustrates that most years with low melt correspond to years with high minimum summer mean bare-ice albedo and vice versa. The direction and the rate of changes in melt rates is mirrored in the minimum summer mean bare-ice albedo (Fig. 6). A negative moderate correlation is also apparent between the mean bare-ice albedo of July, August and September and the respective melt within each month ($\tau = -0.40$). Similarly, a negative moderate correlation is present between the mean bare-ice albedo of individual scenes and daily surface melt ($\tau = -0.43$). These relationships between bare-ice albedo and melt rates across various timescales are illustrated in Appendix A, Fig. 10, and the correlations values between bare-ice albedo and mass balance are provided in Appendix A, Table 3. Appendix A, Fig. 11 depicts the relationship between minimum summer mean bare-ice albedo and glacier-wide annual mass balance. Most years with a positive mass balance correspond to years with high minimum summer mean bare-ice albedo and vice versa (see Appendix A, Fig. 11).

5 DISCUSSION

The bare-ice albedo on Abramov shows a sub-seasonal cycle which reaches its lowest values and variability in August compared with those in July and September. The reduction of albedo between July and August is pronounced at high elevation on the Abramov's tongue, while albedo remains consistently low at the snout. Our results reveal an inverse relationship between seasonal temperature and bare-ice albedo. Yet, a time lag exists between the peak insolation in July, the warmest period from mid-July to mid-August, and the minimum bare-ice albedo at high elevation on the tongue in August. The time lag is likely attributed to elevation-dependent refreezing events in July, which maintain a high and fluctuating albedo at higher elevation. In August, the rise in air temperature along the altitudinal gradient reduces refreezing, leading
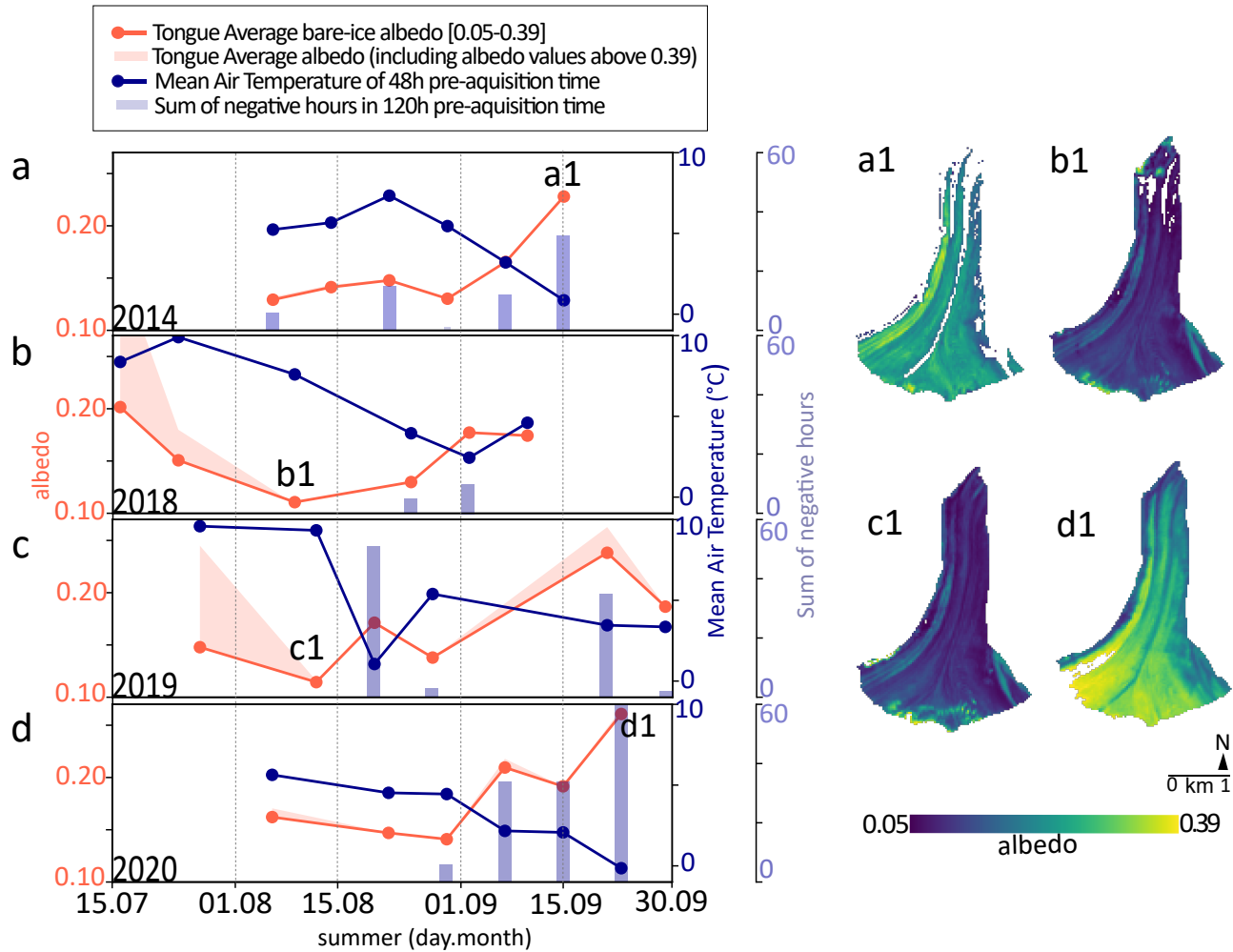
Fig. 5. Average bare-ice albedo over the tongue for each scene (orange line) of (a) 2014, (b) 2018, (c) 2019 and (d) 2020. Average albedo of the tongue, including albedo values above 0.39 for each scene (light orange area) and average air temperature of the 48 h prior to albedo acquisition (dark blue) and sum of negative hours in the 120 h prior to albedo acquisition (light blue) for the four years (a-d). Spatial distribution of bare-ice albedo after cold conditions in a1 (15 September 2014) and d1 (23 September 2020) and after warm conditions in b1 (9 August 2018) and c1 (12 August 2019).

1999–2022 Melt (mm w.e)	Bare-ice albedo (α)	Kendall τ
Summer melt	Summer bare-ice α	-0.40
Summer melt	Summer minimum mean bare-ice α	-0.53
Monthly (Jul, Aug, Sep) melt	Monthly (Jul, Aug, Sep) bare-ice α	-0.40
Daily melt	Average bare-ice α per scene	-0.43
2012–2022 Melt (mm w.e)	Bare-ice albedo (α)	Kendall τ
Summer melt	Summer minimum mean bare-ice α	-0.71

Table 2. Kendall τ between 1999 and 2022 summer melt and mean summer bare-ice albedo over the tongue and summer minimum mean bare-ice albedo over the tongue, between monthly (July, August, September) surface melt and monthly bare-ice albedo over the tongue, between daily surface melt (albedo acquisition dates) and the average bare-ice tongue albedo per scene. Kendall τ between 2012 and 2022 summer melt and summer minimum mean bare-ice albedo over the tongue, corresponding to the in-situ melt measurement period. All relationships are statistically significant at the 99% confidence level with $p - values < 0.01$
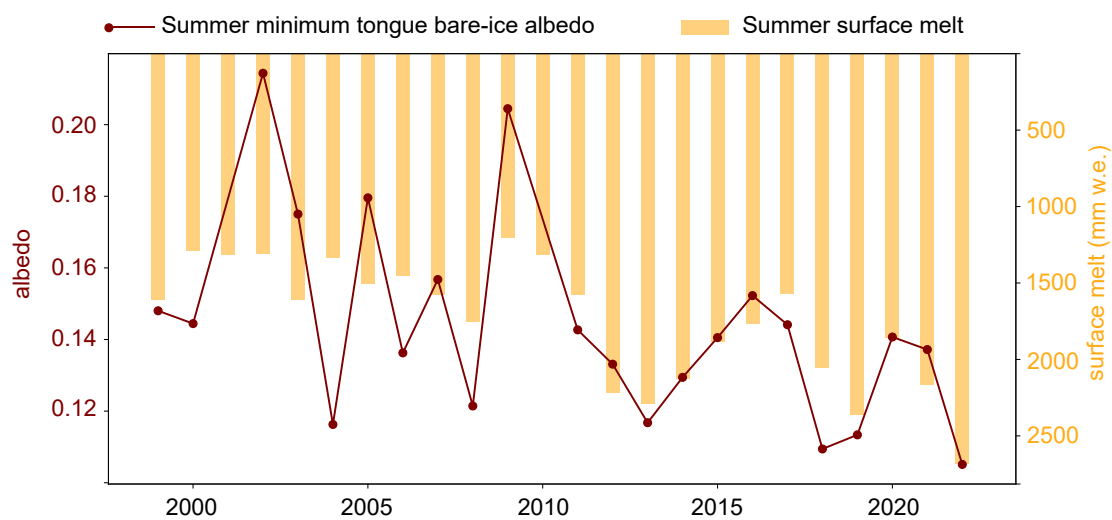
Fig. 6. Summer minimum mean bare-ice albedo over the tongue (dark red) and summer melt (orange) from 1999 to 2022.

to decreased albedo values and variability over the entire tongue. The decrease of albedo between July and August can also be related to prolonged exposure of ice to impurity deposition (Azzoni and others, 2016) and to a decrease in washing-out of impurities by rainfall (Azzoni and others, 2016; Fugazza and others, 2016). Azzoni and others (2016) also observed a disconnection between peak of insolation and the Forni glaciers most intense darkening. The authors relate the phenomena to persisting snow when insolation is strongest. Whereas snow often persists in ogives and crevasses at higher elevation (between 3950 and 4071 m a.s.l.) on Abramovs tongue in July, snow cover changes cannot explain the delay between temperature, insolation and darkening. However, the role of snow in washing-out impurities might contribute to maintain a higher albedo in July. At lower elevation (between 3650 and 3850 m a.s.l.), the tongue of Abramov is preserved from refreezing events and is exposed to warm conditions as early as July, contributing to low and consistent albedo at the snout. This exposure enhances energy inputs to the surface and raises the ice temperature to melting point. The meltwater coating and ponds darken the ice and render it vulnerable to accelerated darkening through the albedo feedback (Paul and others, 2005; Senese and others, 2012; Azzoni and others, 2016).

In September, the rise of bare-ice albedo coincides with reduced sunlight, lower temperature and more negative degree hours. The impact of meltwater on the reflectivity of the ice is reduced, and recurrent refreezing of residual meltwater and weathering crust formation can generate high-reflective ice surfaces (Marshall and Miller, 2020; Tedstone and others, 2020; Barandun and others, 2022). Additionally, the extensive meltwater in August can have washed-out the impurities on the ice and thus increased the albedo for September. The brightening in September is more pronounced on clean ice than on dirty ice because of the reflective properties of clean ice, which quickly generate the necessary conditions for refreezing (Marshall and Miller, 2020).

The trends of bare-ice albedo around the medial moraines reveal a dynamic shift towards the east. This shift is likely the result of changing ice dynamics related to a possible surge initiation in 2018 (Mattea and others, 2023). Lateral displacement and foliations of medial moraines, such as the one on Abramov, have been observed on other surging glaciers (Post, 1972; Wilson and others, 2016; Lovell and Fleming, 2023). The significant trends between 1999 and 2017, unaffected by the glacier dynamics, reveal a widespread darkening of the ice in July, August and September. This darkening is likely related to the atmospheric warming recorded for Central Asia (Parry, 2007), which increases the frequency of melting events, maintains water-coating on the ice for extended periods and suppresses the occurrence of freezing events (Cutler and

Munro, 1996; Naegeli and others, 2019). The darkening of the glacier tongue in July can also be attributed to the earlier onset of melting of the snow cover in the Pamir-Alay (Zhou and others, 2017). This onset results in bare ice exposed to insolation, warm conditions and impurity deposition earlier in the season and for an extended period. The darkening observed at high elevation in September may be related to the gradual delay in the elevation-dependent refreezing events descending over the tongue (Peng and others, 2019).

The detection of potential brightening and darkening of the ice over the full study period remains challenging due to short-term trends and processes that alter the glacier surface. These changes include processes such as the movement of morainic material or the displacement of meltwater streams on the ice. These short-term trends illustrate the importance of observing bare-ice albedo over extended time periods, as underlying darkening of the ice might otherwise be missed.

The progressive darkening of the tongue has critical implications for the melt. The sensitivity of the mass balance to bare-ice albedo variability stems from the crucial role that bare-ice albedo plays in the surface energy budget, triggering melting, thus mass loss and, vice versa, refreezing events that retain mass. These events lead to darkening or brightening phenomena on the ice and contribute to amplified feedback loops of mass loss or gain. The consistency of the correlation between bare-ice albedo and melt over the different time scales highlights that the relationship between the two variables is robust, which indicates that even short-term variability of bare-ice albedo can significantly impact glacier mass loss. Therefore, monitoring bare-ice albedo variability shows potential to provide valuable insights into the response of glaciers to climate change.

Uncertainties

Our results are subject to uncertainties related to the satellite sensor capabilities, the (pre-)processing and the temporal and spatial resolution of the albedo scenes. The Landsat surface reflectance products are reliable for bare-ice albedo analysis on glacier tongues (Naegeli and Huss, 2017; Naegeli and others, 2019; Hartl and others, 2020; Shaw and others, 2021; Barandun and others, 2022). The pre-processing steps applied to the products offer good performance in Naegeli and Huss (2017), who reports strong correlations ($\mathbb{R}^2 = 0.85$) and an absolute average deviation of 0.07 when comparing satellite-retrieved albedo values with in situ measurements. Hartl and others (2020) also found moderate positive correlations in the range of 0.53 and 0.62 between the reflectance measured in-situ and the reflectance values from the different Landsat

bands on bare-ice. The change from Landsat 7 to Landsat 8 might incorporate slight variations in intensity, contrast and coverage between the scenes taken by the two different satellite sensors. However, (Barandun and others, 2022) showed that, despite strong variations over snow albedo, the difference in bare-ice albedo from different Landsat sensors remain very small. The use of scenes from Landsat 7 introduces striping artifacts into the findings in relation to the scan line corrector (SLC) failure (Scaramuzza and others, 2004). The temporal resolution (16 days) of Landsat products provides good coverage for Abramov, but clouds and shadows render multiple scenes unusable, thus limiting the dataset. The temporal distribution of the scenes is uneven, with a strong under-representation of scenes in the initial years of the study period (1999–2012), especially for July and September (see Appendix A, Fig. 8), and an under-representation of pixels in the upper section of the glacier tongue. These issues may have introduced bias in the results of the present study, but their effects were always considered in the interpretation of the analyses.

Filtering of pixels using a definite threshold can lead to mis-classification of surface properties. Naegeli and others (2019) report the critical range (0.25 and 0.55) of albedo values for Landsat products in which investigation is necessary to distinguish snow from ice. We considered camera images and AWS data to identify the snow influence. Moreover, we opted for a conservative approach on the threshold choice and on the filtering procedure. Still, overlap between the albedo of snow and ice occurs. This overlap likely explains why the relationship between temperature and bare-ice albedo is less pronounced for certain dates, such as 16 July 2018 (Fig. 5b). These dates coincide with the presence of snow on the study area (Fig. 5b, c; light orange area), which maintains the mean bare-ice albedo of the tongue in a moderate range, despite high temperatures and despite large areas of very low bare-ice albedo visible on the tongue. The influence of snow cannot be avoided in the analysis despite our conservative bare-ice albedo threshold. This issue is also related to the spatial resolution of optical satellite images. The roughness of the ice surface favours the accumulation of debris and high reflective snow in troughs, thereby influencing pixel-wide albedo values. These small-scale topographic effects cannot be fully avoided in an analysis of moderate resolution optical satellite imagery.

CONCLUSION

The bare-ice albedo of Abramov exhibits sub-seasonal and inter-annual spatio-temporal variability. Changes in air temperature control the temporal variability of bare-ice albedo during the ablation season. We observe inverse correlations between short-term average air temperature and the average bare-ice

albedo on the tongue. Recurrent refreezing at high altitude on the tongue of Abramov is believed to generate the lag between the highest temperatures in July and the lowest average bare-ice albedo in August. Concentrations of impurities, debris and water on the ice dictate the spatial variability of bare-ice albedo during the ablation season. Our results indicate that the albedo of debris-free ice experiences a more pronounced increase than that of the ice in the vicinity of the medial moraines when temperatures and insolation drop from August to September. Bare-ice albedo decreased on Abramov in July and August from 1999 to 2017. These trends are likely related to higher air temperatures and the extension of the snow-free period, both of which can contribute to more frequent and widespread meltwater presence at the glacier surface. Changes in ice dynamics have also occurred on the glacier in the last decade. A lateral displacement of moraines in 2018 suggests that Abramov entered a dynamic phase related to surging activity (Mattea and others, 2023), which is indeed reflected in the albedo values and trends.

Simplified versions of the spatio-temporal variability of bare-ice albedo have been used so far in glaciological modelling (Brock and others, 2000a; Machguth and others, 2006, 2008). Yet, the significant correlations between variations of bare-ice albedo and glacier melt demonstrate the sensitivity of Abramov Glacier to changes of bare-ice albedo. Further research on the drivers of bare-ice albedo variations and the impact of those variations on glacier mass balance are required. With such inputs, bare-ice albedo variations could be integrated effectively into glaciological models to reduce uncertainties in melt modelling and its resulting contribution to river runoff.

6ACKNOWLEDGEMENTS

REFERENCES

Azzoni RS, Senese A, Zerboni A, Maugeri M, Smiraglia C and Diolaiuti GA (2016) Estimating ice albedo from fine debris cover quantified by a semi-automatic method: the case study of Forni Glacier, Italian Alps. *The Cryosphere*, **10**(2), 665–679 (doi: 10.5194/tc-10-665-2016)

Barandun M, Huss M, Sold L, Farinotti D, Azisov E, Salzmann N, Usubaliev R, Merkushkin A and Hoelzle M (2015) Re-analysis of seasonal mass balance at Abramov glacier 19682014. *Journal of Glaciology*, **61**(230), 1103–1117 (doi: 10.3189/2015JoG14J239)

Barandun M, Huss M, Usubaliev R, Azisov E, Berthier E, Kääb A, Bolch T and Hoelzle M (2018) Multi-decadal mass balance series of three Kyrgyz glaciers inferred from modelling constrained with repeated snow line observations. *The Cryosphere*, **12**(6), 1899–1919 (doi: 10.5194/tc-12-1899-2018)

Barandun M, Pohl E, Naegeli K, McNabb R, Huss M, Berthier E, Saks T and Hoelzle M (2021) Hot spots of glacier mass balance variability in Central Asia. *Geophysical Research Letters*, **48**(11), e2020GL092084 (doi: 10.1029/2020GL092084)

Barandun M, Bravo C, Grobety B, Jenk T, Fang L, Naegeli K, Rivera A, Cisternas S, Münster T and Schwikowski M (2022) Anthropogenic influence on surface changes at the Olivares glaciers; Central Chile. *Science of the Total Environment*, **833**, 155068 (doi: 10.1016/j.scitotenv.2022.155068)

Box J, Fettweis X, Stroeve J, Tedesco M, Hall D and Steffen K (2012) Greenland ice sheet albedo feedback: thermodynamics and atmospheric drivers. *The Cryosphere*, **6**(4), 821–839 (doi: 10.5194/tc-6-821-2012)

Braithwaite RJ (1995) Positive degree-day factors for ablation on the Greenland ice sheet studied by energy-balance modelling. *Journal of Glaciology*, **41**(137), 153–160 (doi: 10.3189/S0022143000017846)

Brock BW, Willis IC and Sharp MJ (2000a) Measurement and parameterization of albedo variations at Haut Glacier dArolla, Switzerland. *Journal of Glaciology*, **46**(155), 675–688 (doi: 10.3189/172756500781832675)

Brock BW, Willis IC, Sharp MJ and Arnold NS (2000b) Modelling seasonal and spatial variations in the surface energy balance of Haut Glacier dArolla, Switzerland. *Annals of Glaciology*, **31**, 53–62 (doi: 10.3189/172756400781820183)

Brun F, Dumont M, Wagnon P, Berthier E, Azam MF, Shea JM, Sirguey P, Rabatel A and Ramanathan A (2015) Seasonal changes in surface albedo of Himalayan glaciers from MODIS data and links with the annual mass balance. *The Cryosphere*, **9**(1), 341–355 (doi: 10.5194/tc-9-341-2015)

Cuffey KM and Paterson WSB (2010) *The Physics of Glaciers*. Academic Press

Cutler PM and Munro DS (1996) Visible and near-infrared reflectivity during the ablation period on Peyto Glacier, Alberta, Canada. *Journal of Glaciology*, **42**(141), 333–340 (doi: 10.3189/S0022143000004184)

Davaze L, Rabatel A, Arnaud Y, Sirguey P, Six D, Letreguilly A and Dumont M (2018) Monitoring glacier albedo as a proxy to derive summer and annual surface mass balances from optical remote-sensing data. *The Cryosphere*, **12**(1), 271–286 (doi: 10.5194/tc-12-271-2018)

Denzinger F, Machguth H, Barandun M, Berthier E, Girod L, Kronenberg M, Usubaliev R and Hoelzle M (2021) Geodetic mass balance of Abramov Glacier from 1975 to 2015. *Journal of Glaciology*, **67**(262), 331–342 (doi: 10.1017/jog.2020.108)

Di Mauro B and Fugazza D (2022) Pan-Alpine glacier phenology reveals lowering albedo and increase in ablation season length. *Remote Sensing of Environment*, **279**, 113119 (doi: 10.1016/j.rse.2022.113119)

Dumont M, Gardelle J, Sirguey P, Guillot A, Six D, Rabatel A and Arnaud Y (2012) Linking glacier annual mass balance and glacier albedo retrieved from MODIS data. *The Cryosphere*, **6**(6), 1527–1539 (doi: 10.5194/tc-6-1527-2012)

Emeljyanov YE, Nozdryuhin VK and Suslov VV (1974) The dynamics of the Abramov Glacier during the surge of 19721973 [in Russian]. *Materiali Gljaziologieeskix Issledovanij (Data of Glaciological Studies)*, **24**, 8795

Fallah B, Didovets I, Rostami M and Hamidi M (2024) Climate change impacts on Central Asia: Trends, extremes and future projections. *International Journal of Climatology* (doi: 10.1002/joc.8519)

Fugazza D, Senese A, Azzoni RS, Maugeri M and Diolaiuti GA (2016) Spatial distribution of surface albedo at the Forni Glacier (Stelvio National Park, Central Italian Alps). *Cold Regions Science and Technology*, **125**, 128–137 (doi: 10.1016/j.coldregions.2016.02.006)

Gascoin S, Guðmundsson S, Aðalgeirsdóttir G, Pálsson F, Schmidt L, Berthier E and Björnsson H (2017) Evaluation of MODIS Albedo Product over Ice Caps in Iceland and Impact of Volcanic Eruptions on Their Albedo. *Remote Sensing*, **9**(5), 399 (doi: 10.3390/rs9050399)

Glazyrin GE, Kamnyansky GM and Pertziger FI (1993) *Regime of the Abramov glacier [in Russian]*. Hidrometeoizdat, St. Petersburg

Greuell W and Smeets P (2001) Variations with elevation in the surface energy balance on the Pasterze (Austria). *Journal of Geophysical Research: Atmospheres*, **106**(D23), 31717–31727 (doi: 10.1029/2001JD900127)

Gunnarsson A and Gardarsson SM (2023) Spatial Estimation of Snow Water Equivalent for Glaciers and Seasonal Snow in Iceland Using Remote Sensing Snow Cover and Albedo. *Hydrology*, **11**(1), 3 (doi: 10.3390/hydrology11010003)

Gunnarsson A, Gardarsson SM, Pálsson F, Jóhannesson T and Sveinsson OGB (2021) Annual and inter-annual variability and trends of albedo of icelandic glaciers. *The Cryosphere*, **15**(2), 547–570 (doi: 10.5194/tc-15-547-2021)

Gunnarsson A, Gardarsson SM and Pálsson F (2023) Modeling of surface energy balance for icelandic glaciers using remote-sensing albedo. *The Cryosphere*, **17**(9), 3955–3986 (doi: 10.5194/tc-17-3955-2023)

Hall DK, Ormsby JP, Bindschadler RA and Siddalingaiah H (1987) Characterization of Snow and Ice Reflectance Zones On Glaciers Using Landsat Thematic Mapper Data. *Annals of Glaciology*, **9**, 104–108 (doi: 10.3189/S0260305500000471)

Hartl L, Felbauer L, Schwaizer G and Fischer A (2020) Small-scale spatial variability in bare-ice reflectance at Jamtalferner, Austria. *The Cryosphere*, **14**(11), 4063–4081 (doi: 10.5194/tc-14-4063-2020)

Hoelzle M, Azisov E, Barandun M, Huss M, Farinotti D, Gafurov A, Hagg W, Kenzhebaev R, Kronenberg M, Machguth H and others (2017) Re-establishing glacier monitoring in Kyrgyzstan and Uzbekistan, Central Asia. *Geoscientific Instrumentation, Methods and Data Systems*, **6**(2), 397–418 (doi: 10.5194/gi-6-397-2017)

Hu Z, Zhang C, Hu Q and Tian H (2014) Temperature Changes in Central Asia from 1979 to 2011 Based on Multiple Datasets. *Journal of Climate*, **27**(3), 1143–1167 (doi: 10.1175/JCLI-D-13-00064.1)

Jarvis A, Reuter HI, Nelson A, Guevara E and others (2008) Hole-filled SRTM for the globe Version 4. *available from the CGIAR-CSI SRTM 90m Database (http://srtm. csi. cgiar. org)*, **15**(25-54), 5

Johnson E and Rupper S (2020) An Examination of Physical Processes That Trigger the Albedo-Feedback on Glacier Surfaces and Implications for Regional Glacier Mass Balance Across High Mountain Asia. *Frontiers in Earth Science*, **8**, 129 (doi: 10.3389/feart.2020.00129)

Jonsell U, Hock R and Holmgren B (2003) Spatial and temporal variations in albedo on Storglaciären, Sweden. *Journal of Glaciology*, **49**(164), 59–68 (doi: 10.3189/172756503781830980)

Kendall SM (1975) *Rank Correlation Methods*. Hodder Arnold

Klok EJL and Oerlemans J (2002) Model study of the spatial distribution of the energy and mass balance of Morteratschgletscher, Switzerland. *Journal of Glaciology*, **48**(163), 505–518 (doi: 10.3189/172756502781831133)

Kronenberg M, Machguth H, Eichler A, Schwikowski M and Hoelzle M (2021) Comparison of historical and recent accumulation rates on Abramov Glacier, Pamir Alay. *Journal of Glaciology*, **67**(262), 253–268 (doi: 10.1017/jog.2020.103)

Kronenberg M, van Pelt W, Machguth H, Fiddes J, Hoelzle M and Pertziger F (2022) Long-term firn and mass balance modelling for Abramov Glacier in the data-scarce Pamir Alay. *The Cryosphere*, **16**(12), 5001–5022 (doi: 10.5194/tc-16-5001-2022)

Kruse FA, Lefkoff AB, Boardman JW, Heidebrecht KB, Shapiro AT, Barloon PJ and Goetz AFH (1993) The spectral image processing system (SIPS)interactive visualization and analysis of imaging spectrometer data. *Remote sensing of environment*, **44**(2-3), 145–163 (doi: 10.1016/0034-4257(93)90013-N)

Liang S (2001) Narrowband to broadband conversions of land surface albedo I: Algorithms. *Remote Sensing of Environment*, **76**(2), 213–238, ISSN 0034-4257 (doi: 10.1016/S0034-4257(00)00205-4)

Lovell H and Fleming EJ (2023) Structural evolution during a surge in the Paulabreen glacier system, Svalbard. *Journal of Glaciology*, **69**(273), 141–152 (doi: 10.1017/jog.2022.53)

Machguth H, Paul F, Hoelzle M and Haeberli W (2006) Distributed glacier mass-balance modelling as an important component of modern multi-level glacier monitoring. *Annals of glaciology*, **43**, 335–343 (doi: 10.3189/172756406781812285)

Machguth H, Purves RS, Oerlemans J, Hoelzle M and Paul F (2008) Exploring uncertainty in glacier mass balance modelling with Monte Carlo simulation. *The Cryosphere*, **2**(2), 191–204 (doi: 10.5194/tc-2-191-2008)

Mann HB (1945) Nonparametric Tests Against Trend. *Econometrica: Journal of the Econometric Society*, 245–259

Marshall SJ (2014) Meltwater run-off from Haig Glacier, Canadian Rocky Mountains, 2002–2013. *Hydrology and Earth System Sciences*, **18**(12), 5181–5200 (doi: 10.5194/hess-18-5181-2014)

Marshall SJ and Miller K (2020) Seasonal and interannual variability of melt-season albedo at Haig Glacier, Canadian Rocky Mountains. *The Cryosphere*, **14**(10), 3249–3267 (doi: 10.5194/tc-14-3249-2020)

Mattea E, Machguth H, Berthier E and Hoelzle M (2023) Minor pulsations of Abramov glacier (Kyrgyzstan) observed with multi-sensor optical remote sensing. In *EGU General Assembly Conference Abstracts*, EGU–6296

Mattea E, Berthier E, Dehecq A, Bolch T, Bhattacharya A, Ghuffar S, Barandun M and Hoelzle M (2024) Five decades of Abramov glacier dynamics reconstructed with multi-sensor optical remote sensing. *EGUsphere*, **2024**, 1–43 (doi: 10.5194/egusphere-2024-2169)

Naegeli K and Huss M (2017) Sensitivity of mountain glacier mass balance to changes in bare-ice albedo. *Annals of Glaciology*, **58**(75pt2), 119–129 (doi: 10.1017/aog.2017.25)

Naegeli K, Damm A, Huss M, Schaepman M and Hoelzle M (2015) Imaging spectroscopy to assess the composition of ice surface materials and their impact on glacier mass balance. *Remote Sensing of Environment*, **168**, 388–402 (doi: 10.5167/uzh-98385)

Naegeli K, Huss M and Hoelzle M (2019) Change detection of bare-ice albedo in the Swiss Alps. *The Cryosphere*, **13**(1), 397–412 (doi: 10.5194/tc-13-397-2019)

Oerlemans J (2001) *Glaciers and Climate Change.* CRC Press

Oerlemans J and Knap WH (1998) A 1 year record of global radiation and albedo in the ablation zone of Morteratschgletscher, Switzerland. *Journal of Glaciology*, **44**(147), 231–238 (doi: 10.3189/S0022143000002574)

Parry ML (2007) *Climate Change 2007-Impacts, Adaptation and Vulnerability: Working Group II Contribution to the Fourth Assessment Report of the IPCC*, volume 4. Cambridge University Press

Paterson WSB (1994) *Physics of Glaciers.* Butterworth-Heinemann

Paul F, Machguth H and Kääb A (2005) On the impact of glacier albedo under conditions of extreme glacier melt: The summer of 2003 in the ALPS. *EARSeL eProceedings*, **4**(2), 139–149

Peng D, Zhou T, Zhang L and Zou L (2019) Detecting human influence on the temperature changes in Central Asia. *Climate Dynamics*, **53**, 4553–4568 (doi: 10.1007/s00382-019-04804-2)

Pertziger FI (1996) *Abramov Glacier Data Reference Book: Climate, Runoff, Mass Balance.* Central Asian Regional Research Hydrometeorological Institute, Tashkent, Republic of Uzbekistan

Post A (1972) Periodic Surge Origin of Folded Medial Moraines on Bering Piedmont Glacier, Alaska. *Journal of Glaciology*, **11**(62), 219–226 (doi: 10.3189/S0022143000022218)

Rossini M, Garzonio R, Panigada C, Tagliabue G, Bramati G, Vezzoli G, Cogliati S, Colombo R and Di Mauro B (2023) Mapping Surface Features of an Alpine Glacier through Multispectral and Thermal Drone Surveys. *Remote Sensing*, **15**(13), 3429 (doi: 10.3390/rs15133429)

Scaramuzza P, Micijevic E and Chander G (2004) SLC Gap-Filled Products Phase One Methodology. *Landsat Technical Notes*, **5**

Schaeffer MS and Levitt EE (1956) Concerning Kendall's tau, a nonparametric correlation coefficient. *Psychological Bulletin*, **53**(4), 338 (doi: 10.1037/h0045013)

Schmale J, Flanner M, Kang S, Sprenger M, Zhang Q, Guo J, Li Y, Schwikowski M and Farinotti D (2017) Modulation of snow reflectance and snowmelt from Central Asian glaciers by anthropogenic black carbon. *Scientific Reports*, **7**(1), 40501 (doi: 10.1038/srep40501)

Schöne T, Zech C, Unger-Shayesteh K, Rudenko V, Thoss H, Wetzel HU, Gafurov A, Illigner J and Zubovich A (2013) A new permanent multi-parameter monitoring network in Central Asian high mountains–from measurements to data bases. *Geoscientific Instrumentation, Methods and Data Systems*, **2**(1), 97–111 (doi: 10.5194/gi-2-97-2013)

Senese A, Diolaiuti G, Mihalcea C and Smiraglia C (2012) Energy and Mass Balance of Forni Glacier (Stelvio National Park, Italian Alps) from a Four-Year Meteorological Data Record. *Arctic, antarctic, and alpine research*, **44**(1), 122–134 (doi: 10.1657/1938-4246-44.1.122)

Shaw TE, Ulloa G, Farías-Barahona D, Fernandez R, Lattus JM and McPhee J (2021) Glacier albedo reduction and drought effects in the extratropical Andes, 1986–2020. *Journal of Glaciology*, **67**(261), 158–169 (doi: 10.1017/jog.2020.102)

Suslov V and Krenke A (1980) *Glacier Abramov [in Russian]*. Hydromet Publishing, St. Petersburg

Tedstone AJ, Cook JM, Williamson CJ, Hofer S, McCutcheon J, Irvine-Fynn T, Gribbin T and Tranter M (2020) Algal growth and weathering crust state drive variability in western Greenland Ice Sheet ice albedo. *The Cryosphere*, **14**(2), 521–538 (doi: 10.5194/tc-14-521-2020)

Theil H (1950) A rank-invariant method of linear and polynomial regression analysis. *Indagationes Mathematicae*, **12**(85), 173

Wilson R, Carrión D and Rivera A (2016) Detailed dynamic, geometric and supraglacial moraine data for Glaciar Pio XI, the only surge-type glacier of the Southern Patagonia Icefield. *Annals of Glaciology*, **57**(73), 119–130 (doi: 10.1017/aog.2016.32)

Zhang Y, Gao T, Kang S, Sprenger M, Tao S, Du W, Yang J, Wang F and Meng W (2020) Effects of black carbon and mineral dust on glacial melting on the Muz Taw glacier, Central Asia. *Science of The Total Environment*, **740**, 140056 (doi: 10.1016/j.scitotenv.2020.140056)

Zhou H, Aizen E and Aizen V (2017) Seasonal snow cover regime and historical change in Central Asia from 1986 to 2008. *Global and Planetary Change*, **148**, 192–216 (doi: 10.1016/j.gloplacha.2016.11.011)
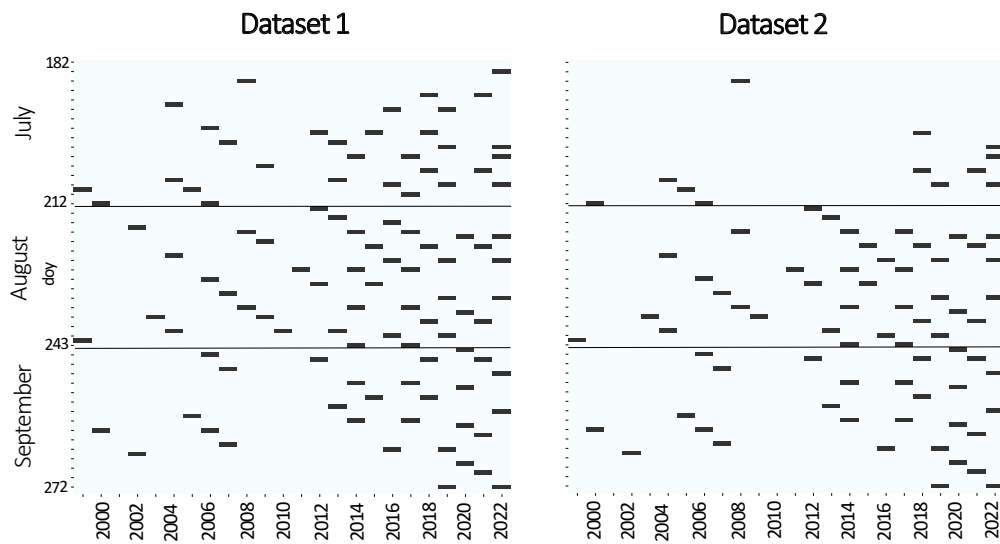
# AAPPENDIX: ADDITIONAL FIGURES AND TABLES
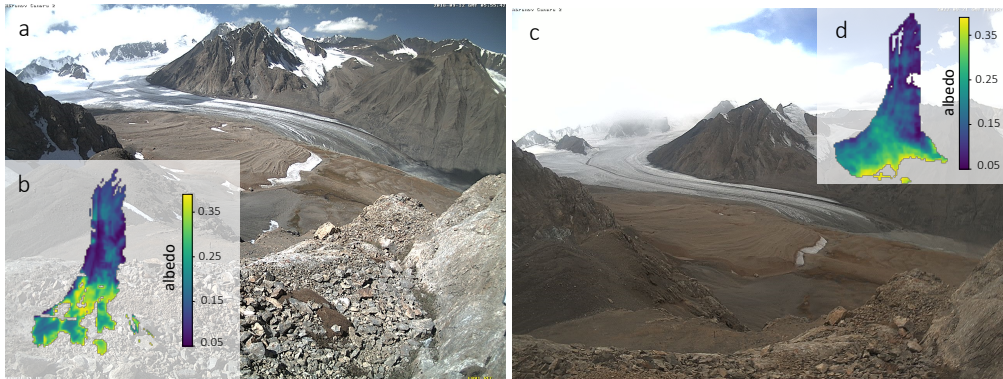
Fig. 7. Examples of images from terrestrial camera 2 at Abramov used for qualitative control and cloud identification are shown in a) for 12 September 2016 and c) for 21 September 2022. The corresponding bare ice albedo distributions for these dates are presented in b) and d), respectively.

Fig. 8. Temporal distribution of satellite scenes acquired during July-August-September (JAS) over the study period (1999-2022)
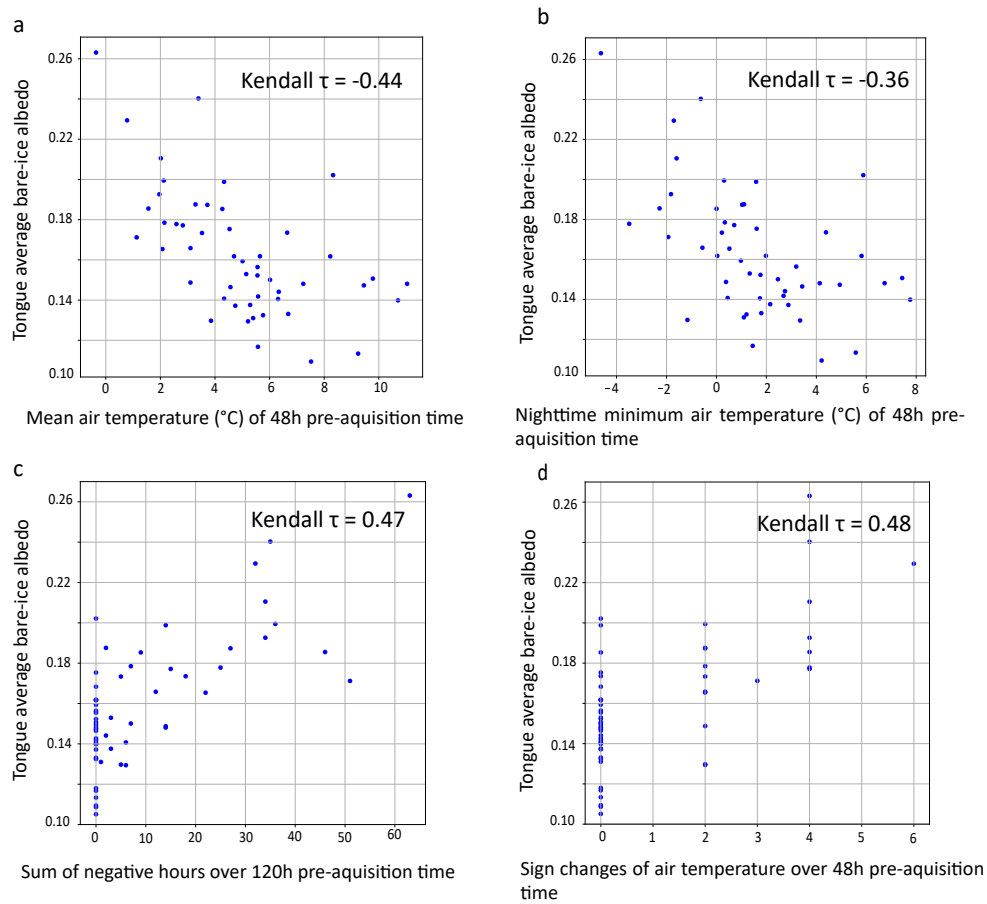
Fig. 9. Relationship between the tongue average bare-ice albedo and a. the mean air temperature over 48h pre-acquisition time b. the minimum nighttime air temperature c. the sum of negative hours over 120h pre-acquisition time d. the sign changes of air temperature over 48h pre-acquisition time.
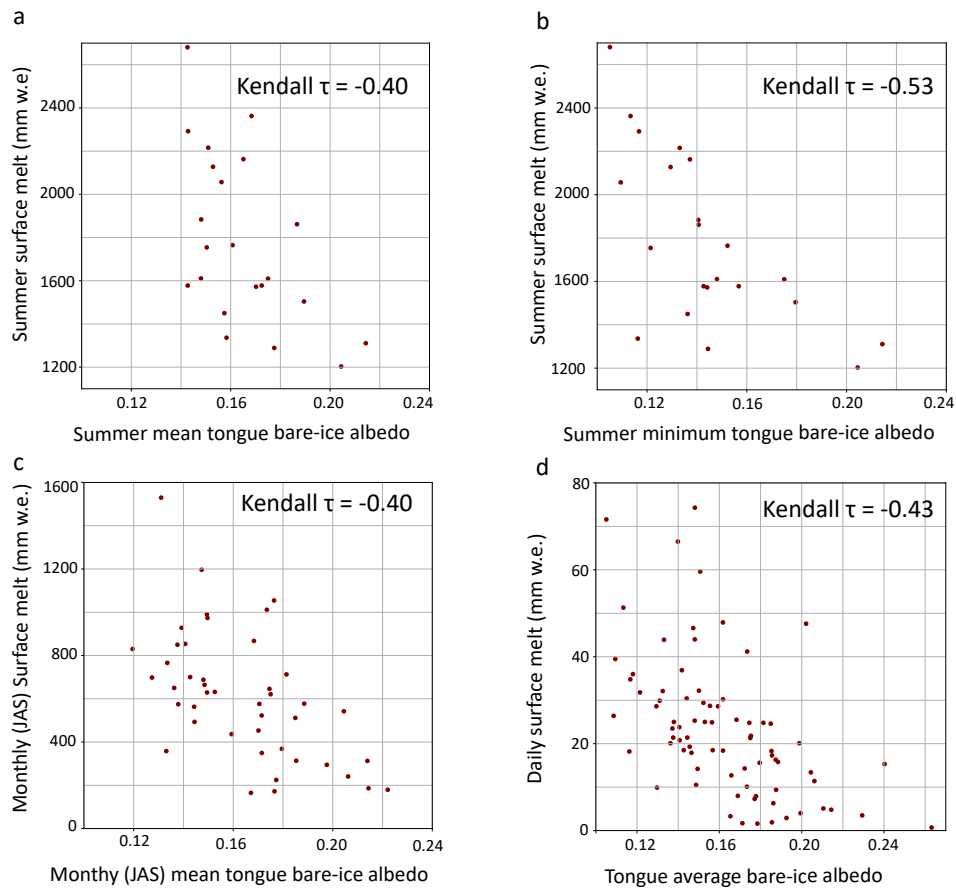
Fig. 10. Relationship between 1999–2022 melt (mm w.e.) and bare-ice albedo. In a. summer melt and mean summer bare-ice albedo b. summer melt and minimum summer bare-ice albedo c. monthly (J,A,S) surface melt and monthly (J,A,S) bare-ice albedo and d. daily surface melt and average bare-ice albedo per scene.

1999–2022 Mass balance (MB)	Bare-ice albedo (α)	Kendall τ
Annual MB	Summer bare-ice α	0.21
Annual MB	Minimum summer bare-ice α	0.55
Monthly (Jul, Aug, Sep) surface MB	Monthly (Jul, Aug, Sep) bare-ice α	0.40
Daily surface MB	Average bare-ice α per scene	0.43

Table 3.   Kendall τ between 1999 and 2022 annual mass balance and mean summer bare-ice albedo over the tongue and minimum summer bare-ice albedo over the tongue, between monthly (July, August, September) surface mass balance and monthly bare-ice albedo over the tongue, between daily surface mass balance (albedo acquisition dates) and the average bare-ice tongue albedo per scene. All relationships are statistically significant at the 95% confidence level with $p-values < 0.05$
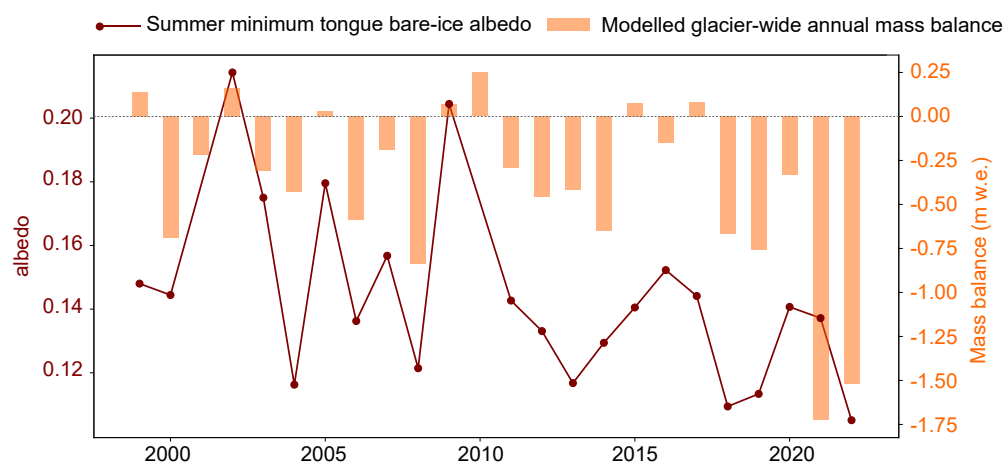
Fig. 11. Minimum summer bare-ice albedo over the tongue (dark red) and glacier-wide annual mass balance (orange) from 1999 to 2022.